SUPPLEMENTARY MATERIAL

Kinetic Competition between Water-Splitting and Photocorrosion Reactions in Photoelectrochemical Devices

Fredy Nandjou[1], Sophia Haussener[1,*]

[1]*Laboratory of Renewable Energy Science and Engineering, EPFL, Station 9, 1015 Lausanne, Switzerland*

Section 1

Energetics and kinetics of charge transfer at the semiconductor-electrocatalyst interface

The presence of catalyst particles on the top of the semiconductor's reacting surface highly impacts the interface physics, influencing not only the charge transfer to the redox couple in solution, but also the charge extraction from the semiconductor.

Figure S1 shows the two main representative designs that can be considered, for a semiconductor (GaAs in this case) that is coated with particle-based electrocatalyst (different from thin-film catalysts).

The first design (Figure S1.a) consists of a layer of electrically non-conductive catalyst particles, which is randomly deposited on the semiconductor surface. In this design, the oxygen evolution reaction occurs at the triple phase (semiconductor-electrocatalyst-electrolyte) boundary. Thus, a single site reaction scheme, which considers the same concentration of reactants (water molecules, holes, etc.) and the same potential for the anodic photocorrosion and oxygen evolution reactions can be applied:

$$\boldsymbol{E}_{\mathbf{EC}} = \boldsymbol{E}_{\mathbf{SC}} = \boldsymbol{E}_{\boldsymbol{p},\mathbf{F}} = \boldsymbol{E}_{\mathbf{VB}} - \boldsymbol{k_B T ln}\left(\frac{\boldsymbol{p}_{\mathbf{SC}}}{\boldsymbol{N}_{\mathbf{VB}}}\right)$$

$$\boldsymbol{p}_{\mathbf{EC}} = \boldsymbol{p}_{\mathbf{SC}}$$

where p_{SC} and p_{EC} stand for the hole concentrations in the semiconductor and electrocatalyst, respectively.

* Corresponding author: sophia.haussener@epfl.ch, +41 21 693 3878

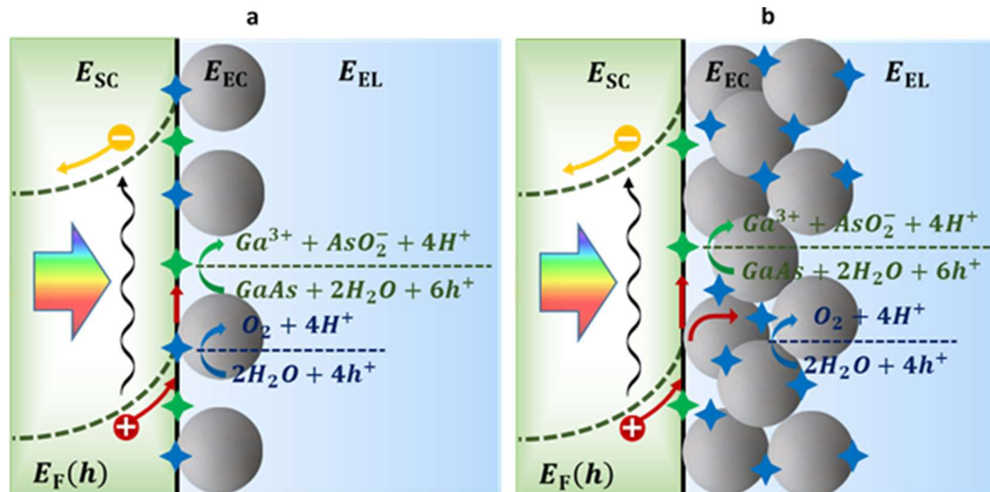

Figure S1. a. Photoelectrode with non-conductive catalyst particles. The oxygen evolution reaction occurs at the triple phase (semiconductor-electrocatalyst-electrolyte) boundary, and a single site reaction scheme can be applied. **b. Photoelectrode with a conductive and porous catalyst layer.** The oxygen evolution reaction occurs over the complete specific surface of the porous structure, and the ion-permeability of the catalyst induces a so called "adaptive junction" [1] . In both cases, the anodic photocorrosion reaction of the semiconductor (GaAs in this case) occurs at the semiconductor-electrolyte interface.

The second design (Figure S1.b) consists of semiconductor covered with a conductive and porous catalyst layer. While the photocorrosion reaction occurs only at the semiconductor-electrolyte interface, the water splitting reaction occurs over the complete specific surface of the porous catalyst layer. With this design, the electrochemically active surface area for water splitting can be maximized. The ion-permeable catalyst induces a so called "adaptive junction" [1] with the semiconductor, where the effective Schottky barrier height changes with the oxidation level of the electrocatalyst. In this case, the impact of energetics and kinetics of the charge transfer from the semiconductor to the electrocatalyst should be taken into account because there are different hole concentrations for the oxygen evolution reaction and anodic photocorrosion reaction, and a potential difference at the semiconductor-electrocatalyst interface.

At equilibrium, the Fermi levels of the semiconductor and electrocatalyst should line up with the electrolyte's potential:

$$E_{EC} = E_{SC} = E_F^0 = E_{CB} + k_B T ln(\frac{n}{N_{CB}})$$

where E_{F}^{0} is the Fermi level in the isolated semiconductor, and n is the electron concentration in the n-type semiconductor.

At non-equilibrium (under the applied photovoltage), the electrocatalyst potential changes *in-situ*, due to the adaptation of the effective Schottky barrier height $\Phi_{\mathrm{B}}^{\mathrm{eff}}$:

$$\boldsymbol{E}_{\mathbf{EC}} = \boldsymbol{E}_{\mathbf{CB}} + \boldsymbol{\Phi}_{\mathbf{B}}^{\mathbf{eff}}$$

The reaction rate for charge transfer at the semiconductor-electrocatalyst interface is given by the following second order rate law [2]:

$$\boldsymbol{R}_{\mathbf{SC/EC}} = \boldsymbol{k}_{\boldsymbol{p}}\left[\boldsymbol{p}_{\mathbf{SC}}[\boldsymbol{M}] - \boldsymbol{p}_{\mathbf{SC}}^{\mathbf{eq}}[\boldsymbol{AB}]\boldsymbol{exp}\left(\frac{\boldsymbol{q}\boldsymbol{E}_{\mathbf{EC}}}{\boldsymbol{k}_{\boldsymbol{B}}\boldsymbol{T}}\right)\right]$$

where k_p is the interfacial charge transfer coefficient at the semiconductor-electrocatalyst interface, p_{SC} is the photogenerated hole concentration at the semiconductor surface, and $p_{\mathrm{SC}}^{\mathrm{eq}}$ is the equilibrium surface concentration of holes when the semiconductor-electrocatalyst junction is formed. $p_{\mathrm{SC}}^{\mathrm{eq}}$ is given by:

$$\boldsymbol{p}_{\mathbf{SC}}^{\mathbf{eq}} = \boldsymbol{p}_{\mathbf{SC}}^{\mathbf{0}}\boldsymbol{exp}\left(\frac{q\boldsymbol{\Phi}_{\mathbf{bi}}}{\boldsymbol{k}_{\boldsymbol{B}}\boldsymbol{T}}\right)$$

where $q\Phi_{\mathrm{bi}} = E_{\mathrm{F}}^{0} - E_{\mathrm{EL}}$ is the built-in voltage, and p_{SC}^{0} is the equilibrium hole concentration in the isolated semiconductor.

In steady-state conditions, the net hole current from the semiconductor to the electrocatalyst matches the net hole current from the electrocatalyst to the redox couple in solution:

$$\boldsymbol{R}_{\mathbf{SC/EC}} = \boldsymbol{R}_{\mathbf{OER}}$$

If we consider the expression of the reaction rate of the OER that was obtained in equations (4) of the manuscript, we obtain:

$$\boldsymbol{k}_{\boldsymbol{p}}\left[\boldsymbol{p}_{\mathbf{SC}}[\boldsymbol{M}] - \boldsymbol{p}_{\mathbf{SC}}^{\mathbf{eq}}[\boldsymbol{AB}]\boldsymbol{exp}\left(\frac{\boldsymbol{q}\boldsymbol{E}_{\mathbf{EC}}}{\boldsymbol{k}_{\boldsymbol{B}}\boldsymbol{T}}\right)\right] = \frac{\overline{\boldsymbol{k}_{\mathbf{1}}}\,\overline{\boldsymbol{k}_{\mathbf{2}}}[\boldsymbol{M}]\boldsymbol{p}_{\mathbf{EC}}{}^{\mathbf{2}}}{\boldsymbol{k}_{-\mathbf{1}} + \overline{\boldsymbol{k}_{\mathbf{2}}}\boldsymbol{p}_{\mathbf{EC}}}$$

where p_{EC} is the hole concentration in the electrocatalyst layer, and $\overline{k_{\iota}}$ are the reaction constants of the oxygen evolution reaction steps, which do not take into account the hole transfer from the semiconductor to the electrocatalyst.

With this interfacial charge transfer model, we obtain different potentials and different hole concentrations for the semiconductor and electrocatalyst, but it implies the appropriate quantification of two additional parameters, that are not well understood: the evolution of the effective Schottky barrier height $\Phi_{\mathrm{B}}^{\mathrm{eff}}$, and the interfacial charge transfer coefficient at the semiconductor-electrocatalyst interface k_p. An evaluation of the effective barrier height was performed by Mills et al. [2] and an evaluation of interfacial charge transfer coefficient at the semiconductor-electrocatalyst interface was performed by Lewis [3]. We used their results to investigate the hole concentration dependence between the electrocatalyst and the semiconductor.

The reference physical properties used in the calculations are listed in Table S1.

Table S1. Reference physical properties used in the calculations.

Physical property	Reference Value	Unit
$\boldsymbol{\Phi_{\mathrm{B}}^{\mathrm{eff}}}$	1.5 [2]	V
$\boldsymbol{E_{\mathrm{Ox}}^{0}}$	1.229	V
$\boldsymbol{E_{\mathrm{Ox}}^{\mathrm{rev}}}$	$E_{\mathrm{Ox}}^{0} - (2.3\ RT/F) \cdot pH$	V
$\boldsymbol{E_{\mathrm{CB}}}$	- 0.9	V
$\boldsymbol{E_{\mathrm{VB}}}$	0.52	V
$\boldsymbol{F}$	96485	C/mol
$\boldsymbol{\overline{k_1^0}}$	10^{-27} [4]	m^4/s
$\boldsymbol{k_{-1}^0}$	10^{-3} [4]	m/s
$\boldsymbol{\overline{k_2^0}}$	10^{-11} [4]	m^4/s
$\boldsymbol{k_p}$	10^{-25} [3]	m^4/s
$\boldsymbol{m_p^*}$	0.5	-
$\boldsymbol{N_{\mathrm{CB}}}$	$4.4 \cdot 10^{23}$	$1/m^3$
$\boldsymbol{N_{\mathrm{VB}}}$	$8.8 \cdot 10^{24}$	$1/m^3$
$\boldsymbol{R}$	8.314	J/mol/K
$\boldsymbol{T}$	300	K

The evolutions of the electrocatalyst hole concentration with the semiconductor hole concentration is given in Figure S2, for different values of k_p. For the parametric study, we considered a variation of k_p between 10^{-27} and 10^{-24} m^4/s.

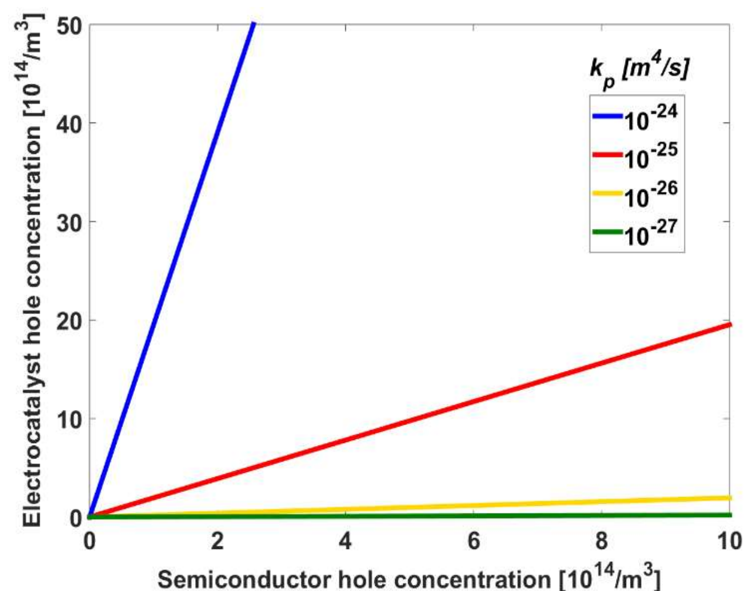

Figure S2. Evolution of the electrocatalyst hole concentration with the semiconductor hole concentration, for different values of the interfacial charge transfer coefficient at the semiconductor-electrocatalyst interface k_p .

We observed that the electrocatalyst hole concentration linearly increased with the semiconductor hole concentration, and the interfacial charge transfer coefficient at the semiconductor-electrocatalyst interface had a considerable impact on the slope. When the rate constant was around 10^{-25} m^4/s (close to the reference value considered by Lewis [3]), both hole concentrations were in the same order of magnitude. For instance, when the hole concentration was $5 \cdot 10^{14}/m^3$ in the semiconductor, it was $\sim 10 \cdot 10^{14}/m^3$ in the electrocatalyst.

The evolutions of the electrocatalyst hole concentration with the semiconductor hole concentration, for different values of the effective barrier height $\Phi_{\mathrm{B}}^{\mathrm{eff}}$, is given in Figure S3. For the parametric study, we considered a variation of $\Phi_{\mathrm{B}}^{\mathrm{eff}}$ between 1.5 and 1.8 V.

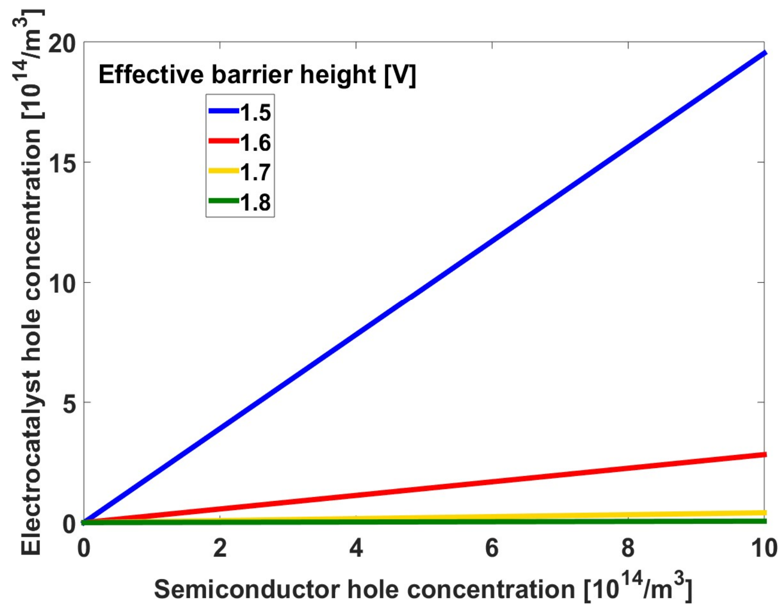

Figure S3. Evolution of the electrocatalyst hole concentration with the semiconductor hole concentration, for different values of the effective barrier height $\Phi_{\mathrm{B}}^{\mathrm{eff}}$.

In this case, it is observed that if the effective barrier height decreased during operation due to adaptation of the junction, the hole concentration in the electrocatalyst considerably increased. For an effective barrier height of around 1.6 V, as measured by Mills et al. [2] during operation, the hole concentration in the electrocatalyst was slightly lower than the one in the semiconductor, even if they were still in the same order of magnitude. For instance, when the hole concentration was $5 \cdot 10^{14}/m^3$ in the semiconductor, it was $\sim 1.5 \cdot 10^{14}/m^3$ in the electrocatalyst.

In summary, the single reaction scheme can be easily applied in the first design presented in Figure S1.a, because the oxygen evolution reaction occurs at the triple phase boundary, and the same hole concentration and potential can be considered for the semiconductor and electrocatalyst particles. For the second design (Figure S1.b), there may be the formation of an adaptive junction. In this case, the dynamics of charge transfer at the semiconductor-electrocatalyst interface need to be known in detail and the relevant parameters need be studied and measured for different semiconductor-catalyst couples. Using our simplified interface model, it appears that the hole concentration in the electrocatalyst and semiconductor should be in the same order of magnitude. These results highly depend on the interfacial charge transfer coefficient at the semiconductor-electrocatalyst interface, and the effective barrier height, two parameters that are still poorly understood.

Globally, the interfacial model that considers the single site reaction scheme (same hole concentration and potential for the semiconductor and electrocatalyst) can be justified, provided that the values of the interfacial charge transfer coefficient at the semiconductor-electrocatalyst interface and the effective barrier height are close to the ones cited in literature [2-3].

Section 2

Evolution of the photostability of different thermodynamically unstable semiconductors, as a function of pH and reaction constant of the rate limiting step of the oxygen evolution reaction.

The plots presented here show the evolution of the photostability as a function of pH and reaction constant of the rate limiting step of the oxygen evolution reaction, k_1^0, for the different thermodynamically unstable semiconductors studied in the main text. The photostability describes the competition between oxygen evolution reaction (OER) and anodic photocorrosion reaction (APR): $\boldsymbol{PS} = \frac{i_{\mathrm{OER}}}{i_{\mathrm{OER}}+i_{\mathrm{APR}}}$. For each studied semiconductor, the pH range is limited to the thermodynamically spontaneous reaction zone for the OER (where $E_{\mathrm{Ox}}(pH) < E_{p,\mathrm{F}}$) and APR (where $E_{p,\mathrm{d}} < E_{\mathrm{Ox}}$). In other words, photoelectrochemical devices that require a bias potential are not considered. Two different values of the photogenerated hole concentrations at the reaction interface are considered (p=10^{10} and 10^{16} holes/m^3). They, for example, highlight the impact of irradiation intensity on photostability. The global input data used for the computation of the photostabiltities are presented in Table S2. These plots can be helpful in determining the operating conditions that are required for photoelectrochemical devices to achieve different levels of photostability.

Table S2. Input data used for the computation of the semiconductors photostability [5-8]. The voltages are referred to NHE.

SC	E_{VB} (V)	E_{VB} shift (V/pH unit)	$E_{p,d}$ (V)	$E_{p,d}$ shift (V/pH unit)	E_{SB} (V)	m_p^*/m_0	n
GaAs	0.52	0	-0.32	-0.059	2.1	0.5	6
GaP	1.1	0	-0.55	-0.059	2.39	0.6	6
InP	0.65	0	-0.24	-0.059	2.05	0.64	6
GaN	2.3	0	-0.66	-0.059	3.2	0.8	6
SiC	1.5	0	-0.25	-0.059	4.65	1	4-8
AlP	1.8	0	-1	-0.059	2.25	0.145	6
AlAs	1.18	0	-1.1	-0.059	2.1	0.22	6
CdTe	0.7	0	0.48	-0.059	1.04	0.6	2
CdS	1.8	0	0.37	-0.059	2.17	0.8	2-4
CdSe	1.3	0	0.73	-0.059	1.33	0.45	2
ZnSe	1.53	0	0.08	-0.059	1.77	0.5	2
ZnS	2.15	0	0.28	-0.059	2.34	0.23	2
PbO	3.25	-0.059	-0.46	0	3.98	2.44	4
SnO	3.74	-0.059	-0.4	0	5.5	0.9	8
WO_3	3.41	-0.059	1.18	0	6.2	2.4	12

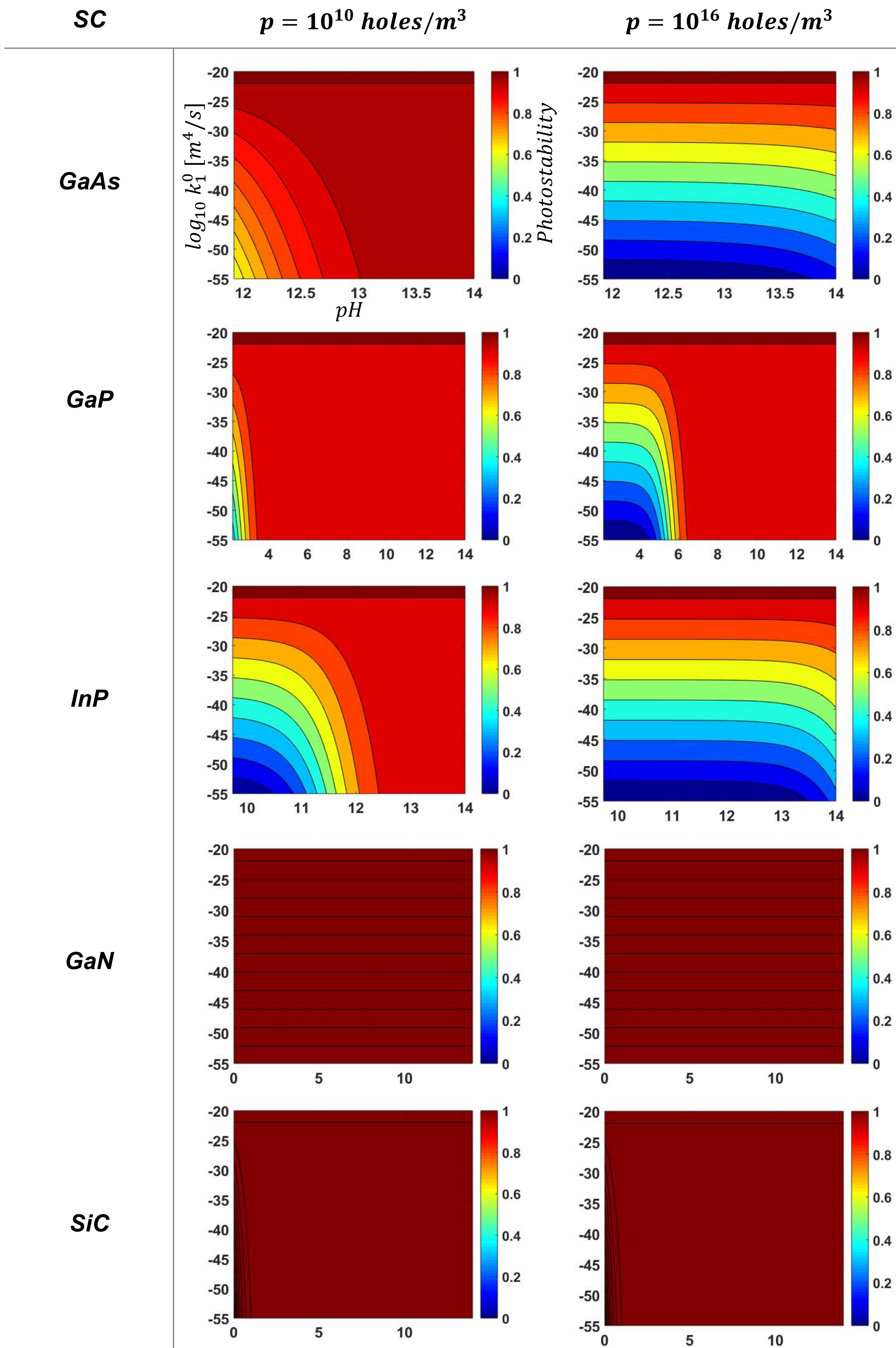
SC
$p = 10^{10}$ $holes/m^3$
$p = 10^{16}$ $holes/m^3$
GaAs
GaP
InP
GaN
SiC
$log_{10}\, k_1^0\ [m^4/s]$
pH
$Photostability$

SC	$p = 10^{10}\ holes/m^3$	$p = 10^{16}\ holes/m^3$
AlP	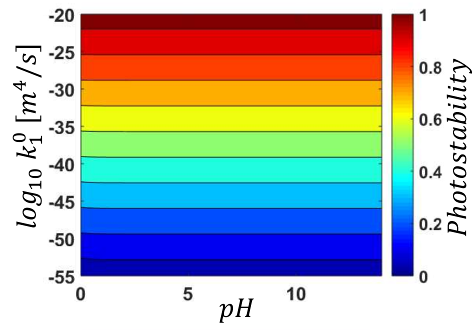	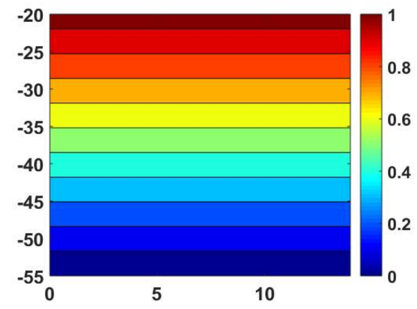
AlAs	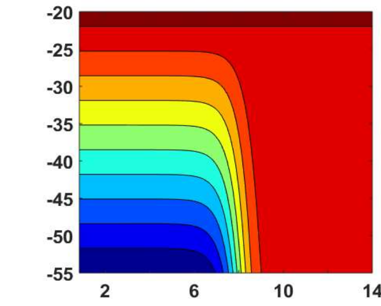	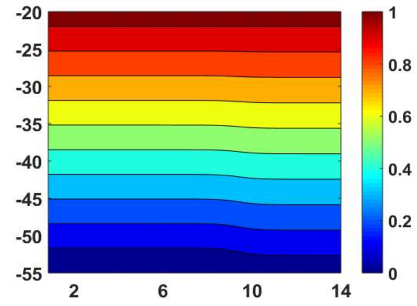
CdTe	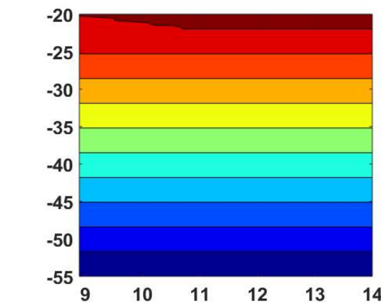	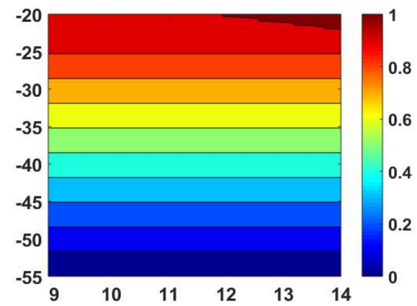
CdS	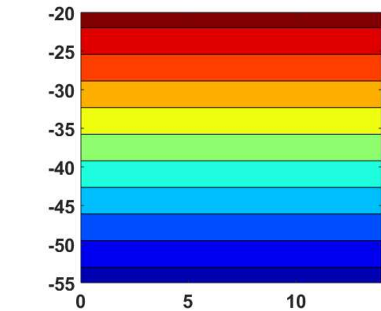	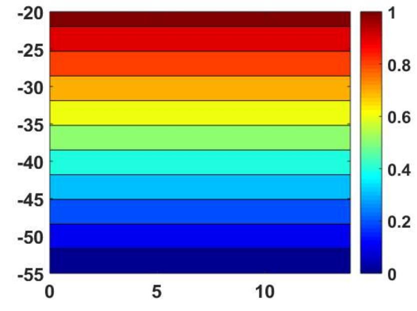
CdSe	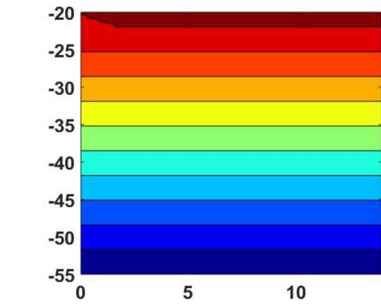	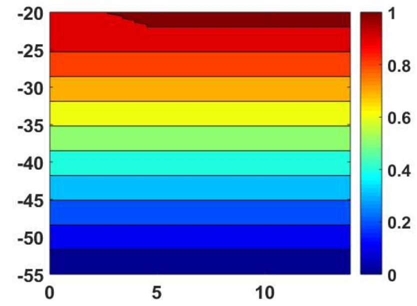

SC	$p = 10^{10}\ holes/m^3$	$p = 10^{16}\ holes/m^3$
ZnSe	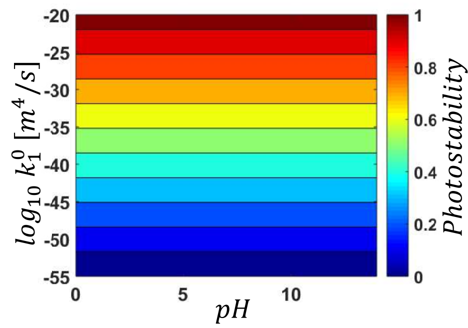	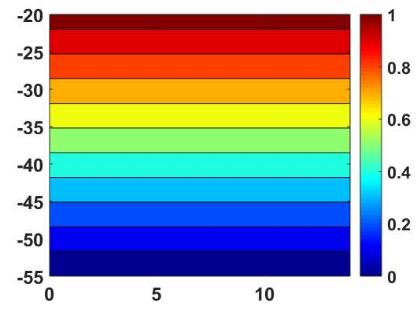
ZnS	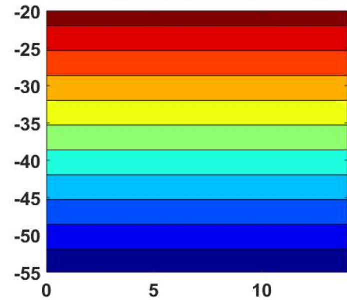	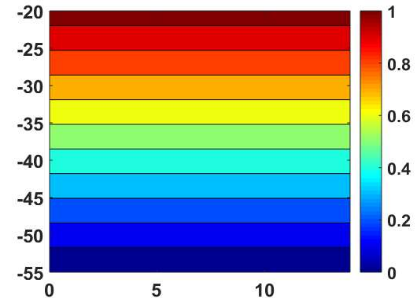
PbO	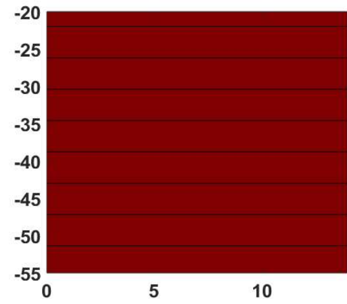	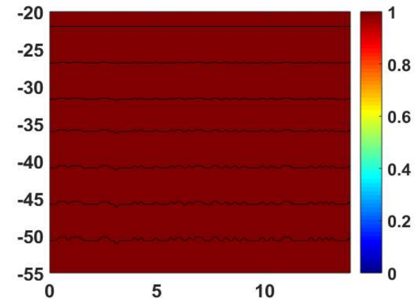
SnO	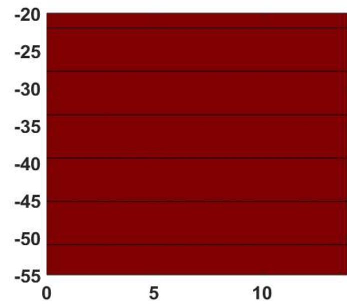	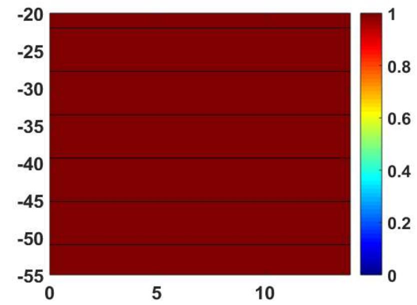
WO_3	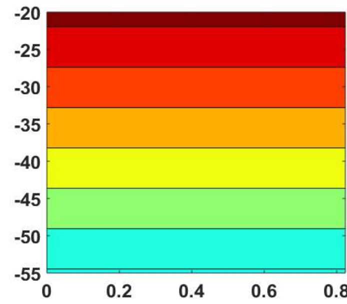	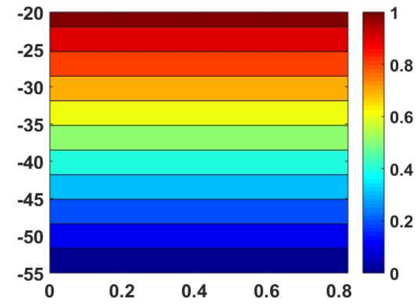

References

[1] F. Lin, S. W. Boettcher, *Nature Materials* **2014**, 13, 81-86.

[2] T. J. Mills, F. Lin, S. W. Boettcher, *Phys. Rev. Lett*. **2014**, 112, 148304.

[3] N. S. Lewis, *Inorganic Chemistry* **2005**, 44, 6900-6911.

[4] P. Allongue, S. Blonkowski, *J. Electroanal. Chem.* **1991**, 316, 57–77.

[5] S. Chen, L. W. Wang, *Chem. Mater.* **2012**, 24, 3659–3666.

[6] Y. R. Luo, *J. Am. Chem. Soc.* **2004**, 126, 982–982.

[7] D. A. Garcia-Osorio, R. Jaimes, J. Vazquez-Arenas, R. H. Lara, J. Alvarez-Ramirez, *J. Electrochem. Soc.* **2017**, 164, E3321–E3328.

[8] R. Memming, *Semiconductor Electrochemistry* (WILEY-VCH Verlag GmbH) **2012**.